

A wavelet finite element-based adaptive-scale damage detection strategy

Wen-Yu He¹, Songye Zhu^{*1} and Wei-Xin Ren²

¹Department of Civil and Environmental Engineering, The Hong Kong Polytechnic University, Hung Hom, Kowloon, Hong Kong

²School of Civil Engineering, Hefei University of Technology, Hefei 230009, China

(Received July 18, 2012, Revised May 28, 2013, Accepted June 24, 2013)

Abstract. This study employs a novel beam-type wavelet finite element model (WFEM) to fulfill an adaptive-scale damage detection strategy in which structural modeling scales are not only spatially varying but also dynamically changed according to actual needs. Dynamical equations of beam structures are derived in the context of WFEM by using the second-generation cubic Hermite multiwavelets as interpolation functions. Based on the concept of modal strain energy, damage in beam structures can be detected in a progressive manner: the suspected region is first identified using a low-scale structural model and the more accurate location and severity of the damage can be estimated using a multi-scale model with local refinement in the suspected region. Although this strategy can be implemented using traditional finite element methods, the multi-scale and localization properties of the WFEM considerably facilitate the adaptive change of modeling scales in a multi-stage process. The numerical examples in this study clearly demonstrate that the proposed damage detection strategy can progressively and efficiently locate and quantify damage with minimal computation effort and a limited number of sensors.

Keywords: damage detection; adaptive-scale; wavelet finite element model; cubic Hermite multiwavelets; modal strain energy

1. Introduction

Structural health monitoring (SHM) systems have been gaining worldwide popularity in the past two decades. In particular, substantial research has been focused on vibration-based damage detection approaches among a wide variety of SHM techniques (Doebeling *et al.* 1996, Sohn *et al.* 2004, Balageas *et al.* 2006, Fan and Qiao 2011). The damage-induced change in dynamic characteristics has been extensively used to locate and quantify structural damage, where the typical dynamic characteristics include frequencies, mode shapes, damping, mode shape curvatures, and strain mode shapes, and their representative derivatives include the modal assurance criterion, frequency response function, modal strain energy, energy transfer ratio, and flexibility matrix, among others. Many of these methods rely on the analytical finite element model (FEM) of a structure, which serves as a relationship model between sensor measurement and unobserved structural responses. The accuracy of FEM often affects the success of damage

*Corresponding author, Ph.D., E-mail: ceszhu@polyu.edu.hk

detection.

However, a dilemma exists in these FEM-based damage detection methods: On one hand, a delicate FEM with fine details is required to obtain high-resolution dynamic properties of structures to enable the identification of minor or localized damages; on the other hand, excessive meshing density of FEM is often impractical, if not impossible, in damage detection of large-scale civil structures, because a significant number of degree of freedoms (DOFs) render damage detection problems time consuming and even ill conditioned. Moreover, owing to sensor noise or the limited number of sensors, only low frequencies and mode shapes can be identified through *in situ* test data. An excessively dense meshing of FEM may not be necessary in this situation. Therefore, a multi-scale FEM is desirable for the damage detection purpose with high resolution at the critical locations and relatively low resolution elsewhere.

The concept of using multi-scale FEM in damage detection has been embraced by several researchers. Ding *et al.* (2010) developed a multi-scale FEM of a long-span cable-stayed bridge, and their analysis results well correlated with the measured dynamic properties from ambient vibration tests. Li *et al.* (2009) proposed a multi-scale modeling strategy for structural deterioration analysis in which a “large-scale” model is adopted for the global responses of structures with linear behavior and a “small-scale” model is available for nonlinear damage analysis of the local welding. A substructuring method in which a complete structure was divided into several substructures has also been used for multi-scale damage identification, and the analysis focused on a substructure with a small number of DOFs (Perera and Ruiz 2008). Bakhary *et al.* (2010) proposed a damage detection approach based on a multi-stage artificial neural network model and progressive substructure zooming. To improve damage detection efficiency and accuracy, several multi-step damage detection processes have been presented, such as “location—quantification” (Shi *et al.* 2000, 2002), “identify general area of structural damage—locate a specific damaged structural component” (Kim and Bartkowicz 1997), “identify damage occurrence—classify damage type—locate and quantify damage” (Kim *et al.* 2010).

Damage detection can greatly benefit from a multi-resolution FEM in that such an approach helps achieve an appropriate tradeoff between modeling details and entirety, as well as between computation accuracy and efficiency. However, a practical challenge arises from the fact that the probable damage locations and the required modeling resolutions are often unpredictable, and thus *a priori* finite element meshing based on analytical simulations or empirical estimates may not be appropriate. Therefore, an ideal damage detection strategy should be based on an adaptive-scale modeling technique that enables us to examine a structure in its entirety, detect the suspected region using a low-resolution model, and then identify the accurate location and severity of the damage with localized refinement in the suspected region only. However, the implementation of such adaptive-scale models in the context of traditional FEM is still a difficult task. Re-meshing a local region requires re-constructing stiffness and mass matrices, as well as repeating the entire computation process. As the desirable scales need to be determined by iteration, the damage detection process becomes computation intensive, especially for large-scale civil structures.

In view of this, this paper proposes an adaptive-scale damage detection approach based on wavelet finite element models (WFEMs). The WFEM is a powerful FEM technique with unique multi-resolution and localization properties that has been developed in recent years (Ko *et al.* 1995, Chen and Wu 1995, Sudarshan and Amaratunga 2003, Han *et al.* 2005, 2006, Amaratunga and Sudarshan 2006, He *et al.* 2012, He and Ren 2012, 2013a, b). Its resolution can be modified conveniently to improve the required analysis accuracy, which is particularly suitable for adaptive-scale damage detection. Some researchers have used the WFEM for the damage detection

of beams by establishing a database of the natural frequency—crack parameter relationship (Li *et al.* 2005, Chen *et al.* 2006, Xiang *et al.* 2006, Xiang and Liang 2011). However, those papers only used WFEM to carry out modal analysis and demonstrate its high computation efficiency. The most important multi-resolution and localization features of WFEM that would be useful for adaptive structural analysis and damage localization were not studied. The current paper adopts a progressive damage detection process in which problems are analyzed in coarse mesh first and better approximation can be subsequently acquired by high-resolution refinement in the concerned regions. Second-generation cubic Hermite multiwavelets are used as shape functions of beam elements, and the change ratio of modal strain energy is used as an indicator of the damage location. A damage matrix equation deduced from the equation of motion of a beam structure through modal perturbation is then used to quantify the severity of the damage. The proposed approach can locate and quantify sub-element damage in beam structures in a progressive manner. Numerical examples of a simply supported beam and a continuous beam with different damage scenarios are simulated in consideration of the effect of random noise. The results clearly demonstrate the effectiveness and accuracy of the proposed adaptive-scale damage detection approach. Compared with traditional methods, fewer DOFs in FEM and fewer sensors in modal tests are involved, thereby considerably enhancing both computation and test efficiency.

2. Theory of multi-scale WFEM

2.1 Wavelet-based multi-resolution analysis

Multi-resolution analysis (MRA) is one of the most important properties of wavelets (Mallat 1988, Chui 2009). Any function $f(x) \in L^2(R)$ can be approximated with different levels of precision in the corresponding space V_j , where the approximation space V_j is spanned by the scaling functions $\phi_{j,l}$. The subscripts j and l define the scale and shift of the scaling functions, respectively (Mallat 1988)

$$\phi_{j,l}(x) = \phi[2^j(x-l)] \quad (1)$$

For example, function $f(x)$ can be approximated in V_0 as follows

$$f(x) \approx f^0(x) = \sum_l a_{0,l} \phi_{0,l} \quad (2)$$

where $\phi_{0,l}$ is the scaling function (also called father wavelet) at scale 0, and $a_{0,l}$ represents the corresponding wavelet coefficient

$$a_{0,l} = \langle f(x), \phi_{0,l}(x) \rangle \quad (3)$$

The accuracy of approximation can be improved by adding terms in the space W_0 , which is the orthogonal complement of V_0 . As a result, the approximation in space V_1 is

$$f(x) \approx f^1(x) = \sum_l a_{0,l} \phi_{0,l} + \sum_m b_{0,m} \psi_{0,m} \quad (4)$$

where $\psi_{0,m}$ is the wavelet function (also called mother wavelet) at scale 0, and $b_{0,m}$ is the

corresponding wavelet coefficients in space W_0 .

$$b_{0,m} = \langle f(x), \psi_{0,m}(x) \rangle \quad (5)$$

With further increase in the approximation order, the wavelet representation of the function approaches to the exact function when $j \rightarrow \infty$.

$$f(x) \approx f^j(x) = \sum_l a_{0,l} \phi_{0,l} + \sum_j \sum_m b_{j,m} \psi_{j,m}, \quad f(x) = f^{j \rightarrow \infty}(x) \quad (6)$$

2.2 Fundamentals of the WFEM

The multi-scale WFEM is the fundamental of the adaptive-scale detection method of structural damage, and a brief introduction to the WFEM is provided in this section. In the WFEM, the shape function of an element uses the wavelet approximation shown in Eq. (6). A variety of wavelets have been used in WFEMs, such as Daubechies wavelets (Ko *et al.* 1995, Chen *et al.* 2006), spline wavelets (Chen and Wu 1995, Han *et al.* 2006, Xiang *et al.* 2006), trigonometric wavelets (He *et al.* 2012, He and Ren 2012, 2013a, b), Hermite wavelets (Xiang and Liang 2011, Wang *et al.* 2011), and so on. The types of elements include the truss element (Wang *et al.* 2011), Timoshenko beam element (Wang *et al.* 2011), Euler-Bernoulli beam element (Han *et al.* 2005, 2006, He and Ren 2012, 2013a), plate element (Han *et al.* 2006), solid element (Han *et al.* 2006) and so on. Its localization characteristics make the WFEM a powerful tool to analyze fields with gradient changes or singularities, such as material nonlinearity, local damage, and cracks. The refinement relations of the scaling functions and wavelets in two adjacent scales are expressed as follows (Chui 2009)

$$\phi_{j,k} = \sum_l h_{j,k,l} \phi_{j+1,l} \quad (7)$$

$$\psi_{j,m} = \sum_l g_{j,m,l} \phi_{j+1,l} \quad (8)$$

where $\phi_{j,k} : k \in K(j)$ represents the vector of multi-scaling functions at the j th scale, $\psi_{j,m} : m \in M(j)$ represents the vector of multiwavelets at the j th scale, and $h_{j,k,l}$ and $g_{j,m,l}$ are the low-pass and high-pass filters, respectively.

Due to its favorable localization characteristics and convenient integral operation, the beam-type element based on second-generation cubic Hermite multiwavelets constructed by Wang *et al.* (2011) is adopted for the damage detection of beam structures in this study. When defined on the interval $[-1, 1]$, the scaling functions consist of two cubic Hermite splines

$$\phi_{0,0} = [\phi_{0,0}^1(x) \quad \phi_{0,0}^2(x)]^T \quad (9)$$

where

$$\phi_{0,0}^1(x) = \begin{cases} (x+1)^2(-2x+1) & x \in [-1,0] \\ (x-1)^2(2x+1) & x \in [0,1] \\ 0 & \text{otherwise} \end{cases} \quad (10)$$

$$\phi_{0,0}^2(x) = \begin{cases} (x+1)^2x & x \in [-1,0] \\ (x-1)^2x & x \in [0,1] \\ 0 & \text{otherwise} \end{cases} \quad (11)$$

The refinement coefficients $h_{j,k,l}$ can be computed by solving simultaneous Eq. (7) at random vertices. The refinement relation of the cubic Hermite scaling functions between two adjacent scales j and $j+1$ reads

$$\phi_{j,k_2} = \phi_{j+1,k_2} + \begin{bmatrix} \frac{1}{2} & \frac{3}{2h} \\ -\frac{h}{8} & -\frac{1}{4} \end{bmatrix} \phi_{j+1,m_1} + \begin{bmatrix} \frac{1}{2} & -\frac{3}{2h} \\ \frac{h}{8} & -\frac{1}{4} \end{bmatrix} \phi_{j+1,m_2} \quad (12)$$

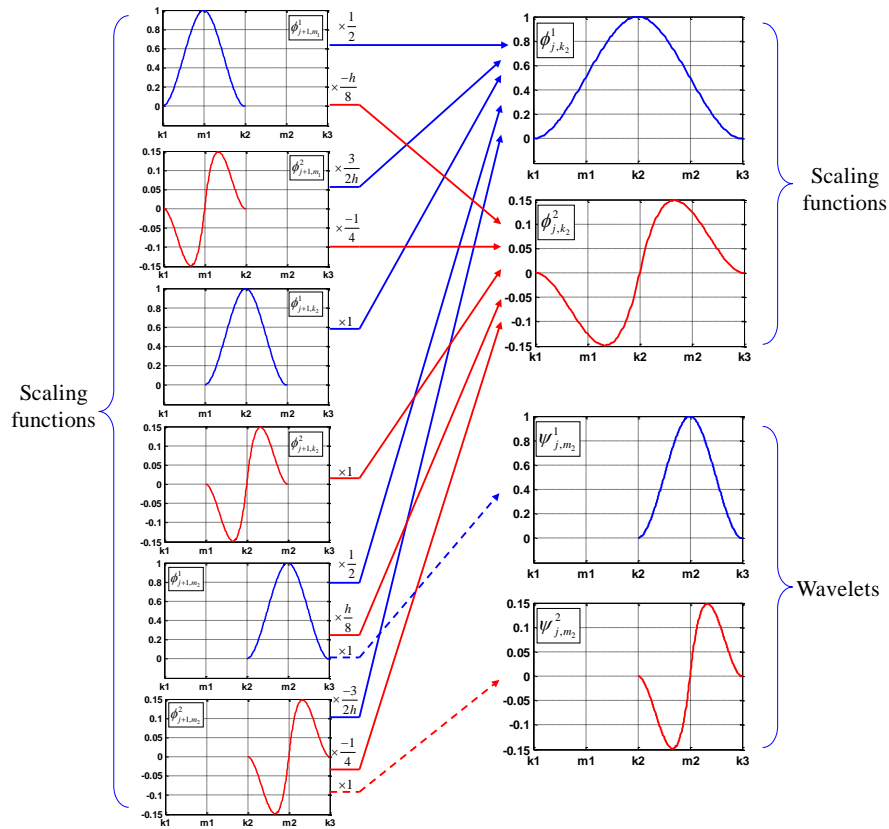


Fig. 1 The refinement relation for cubic Hermite scaling functions

Fig. 1 shows the refinement relation of the cubic Hermite scaling functions defined in Eq. (12). The scaling function ϕ_{j,k_2} has a compact support on $[k_1, k_3]$, whereas the scaling function ϕ_{j+1,k_2} is compactly supported on $[m_1, m_2]$, only a half interval of that at scale j ; h is the length of the interval $[k_1, k_3]$.

The wavelets corresponding to the cubic Hermite scaling functions are not unique. Several cubic Hermite wavelet functions have been previously derived (Sudarshan and Amaratunga 2003, Averbuch *et al.* 2007, Wang *et al.* 2011). For example, Sudarshan and Amaratunga (2003) constructed cubic Hermite wavelets with four vanishing moments using the lifting scheme proposed by Sweldens (1996). Another simple form of cubic Hermite wavelets was constructed and used by Averbuch *et al.* (2007), Wang *et al.* (2011), He and Zhu (2013)

$$\psi_{j,m_2} = \phi_{j+1,m_2} \tag{13}$$

These multiwavelets are adopted in this study because of their simplicity and relatively short support length. The wavelets are compactly supported on the interval between two adjacent k -nodes, e.g., $[k_2, k_3]$. The Hermite scaling functions and wavelets have two DOFs at each node, namely, displacement and rotation DOFs.

In Wang *et al.* (2011), only static equations and the corresponding lifting scheme are presented for beam structures. As the modal properties of structures are often needed in system identification or damage detection, the dynamic equations of beam structures and the corresponding lifting scheme are derived in this study for the aforementioned multi-scale WFEM. According to the classic theory of Euler-Bernoulli beams, the generalized function of potential energy for free vibration is calculated as follows (Zienkiewicz and Taylor 1961)

$$\Pi_p(w) = \int_0^l \frac{EI(x)}{2} \left(\frac{d^2w}{dx^2}\right)^2 dx - \frac{1}{2} \int_0^l \lambda \rho w^2 dx \tag{14}$$

where l is the beam length, ρ is the mass per unit length, λ is the vibration eigenvalue, w is the deflection, and EI is the flexural rigidity. The unknown field w can be approximated by the scaling and wavelet functions of the cubic Hermite multiwavelets

$$w = \sum_k a_{0,k} \phi_{0,k} + \sum_j \sum_m b_{m,j} \psi_{m,j} = \Phi_0 \mathbf{a} + \Psi_0 \mathbf{b}_0 + \Psi_1 \mathbf{b}_1 \cdots + \Psi_{j-1} \mathbf{b}_{j-1} = \Phi_j \mathbf{C}_j \tag{15}$$

where Φ_0 represents the scaling functions at scale 0, and Ψ_j represents the wavelets at scale j , $\Phi_j = [\Phi_0^T, \Psi_0^T, \Psi_1^T \cdots \Psi_{j-1}^T]$ is a row vector of scaling and wavelet functions, and $\mathbf{C}_j = [\mathbf{a}; \mathbf{b}_0; \mathbf{b}_1; \cdots; \mathbf{b}_{j-1}]$ is a column vector of the undetermined wavelet coefficients, which can be regarded as the general DOFs in the wavelet finite element space. Substituting Eq. (15) into Eq. (14) leads to

$$\Pi_p(w) = \int_0^l \frac{EI(x)}{2l^3} \mathbf{C}_j^T (\Phi_j'')^T (\Phi_j'') \mathbf{C}_j d\xi - \frac{1}{2} \int_0^l \lambda \rho \mathbf{C}_j^T \Phi^T \Phi \mathbf{C}_j d\xi \tag{16}$$

where Φ_j'' represent the second derivatives of Φ with respect to the local coordinate ξ . To minimize the potential energy by letting $\delta \Pi_p = 0$, the free vibration formulations of beam elements

at scale j can be obtained as follows

$$(\mathbf{K}_j - \lambda \mathbf{M}_j) \mathbf{C}_j = 0 \tag{17}$$

where λ and \mathbf{C}_j are the eigenvalues and eigenvectors corresponding to the DOFs in the wavelet finite element space, respectively; and \mathbf{K}_j and \mathbf{M}_j are the element stiffness and mass matrices at scale j , respectively:

$$\mathbf{K}_j = \frac{EI}{l^3} \int_0^1 (\Phi_j'')^T (\Phi_j'') d\xi = \frac{EI}{l^3} \int_0^1 \begin{bmatrix} (\Phi_0'')^T (\Phi_0'') & (\Phi_0'')^T (\Psi_0'') & \cdots & (\Phi_0'')^T (\Psi_{j-1}'') \\ & (\Psi_0'')^T (\Psi_0'') & \cdots & (\Psi_0'')^T (\Psi_{j-1}'') \\ \text{sym} & & \ddots & \vdots \\ & & & (\Psi_{j-1}'')^T (\Psi_{j-1}'') \end{bmatrix} d\xi \tag{18}$$

$$\mathbf{M}_j = \rho l \int_0^1 \Phi_j^T \Phi_j d\xi = \rho l \int_0^1 \begin{bmatrix} \Phi_0^T \Phi_0 & \Phi_0^T \Psi_0 & \cdots & \Phi_0^T \Psi_{j-1} \\ & \Psi_0^T \Psi_0 & \cdots & \Psi_0^T \Psi_{j-1} \\ \text{sym} & & \ddots & \vdots \\ & & & \Psi_{j-1}^T \Psi_{j-1} \end{bmatrix} d\xi \tag{19}$$

Due to the orthogonality of the selected cubic Hermite scaling functions and wavelets, the non-diagonal sub-matrices of Eq. (18) become zeros and the stiffness matrix is thus scale decoupled (Wang *et al.* 2011)

$$\mathbf{K}_j = \frac{EI}{l^3} \int_0^1 (\Phi_j'')^T (\Phi_j'') d\xi = \frac{EI}{l^3} \int_0^1 \begin{bmatrix} (\Phi_0'')^T (\Phi_0'') & & & \\ & (\Psi_0'')^T (\Psi_0'') & & \\ & & \ddots & \\ & & & (\Psi_{j-1}'')^T (\Psi_{j-1}'') \end{bmatrix} d\xi \tag{20}$$

Although the mass matrix \mathbf{M}_j is not scale decoupled, the matrix \mathbf{M}_j can be completely retained in the lifting procedure from scale j to scale $j+1$, and only new rows and columns are added into the existing matrix. Unlike in conventional FEM, the mass and stiffness matrices in WFEM can be conveniently updated upon refinement without re-meshing the structures and re-constructing the entire matrices. In addition, the new results after refinement can be readily obtained via iteration with the initial values equal to the results at the last scale. This merit of the Hermite WFEM renders the computation in the refinement process more efficient, and makes the adaptive-scale modelling technique more effective in damage detection where the desirable modelling scales are *a priori* unknown and need to be dynamically and conveniently changed according to different damage scenarios.

The eigenvectors \mathbf{C}_j represent the mode shapes expressed in the wavelet finite element space. Although the mode shapes obtained in modal testing are always expressed in general DOFs, they can be conveniently converted into wavelet DOFs using the Hermite interpolation properties of the adopted multiwavelets. The physical meaning of wavelet DOFs (or coefficients) differs from that of traditional DOFs of nodes. However, adding high scales in the wavelet space is equivalent to adding new interior DOFs within the original element. This is analogous to the mesh refinement in

conventional FEM, but with much simpler operations.

3. Adaptive-scale damage detection

Damage detection methods based on modal strain energy have been extensively explored in the context of traditional FEM in SHM (Shi and Law 1998, Cornwell *et al.* 1999, Shi *et al.* 2000, Guan and Karbhari 2008, Yan *et al.* 2010, 2012). Therefore, modal strain energy is also adopted in the damage detection in the present study. As the strategy described in this work aims to identify damage with a size smaller than a beam element, it uses the modal strain energy in a sub-element. In addition, the elemental modal strain energy in traditional FEM can be calculated as the combination of mode shape vector and element stiffness matrix (e.g., Shi and Law 1998, Shi *et al.* 2000, 2002), while the modal strain energy of a given sub-division in the WFEM cannot be calculated in this direct way. Thus, the sub-element partial differential equation governing free vibration of a beam is used in the formulation of damage quantification matrix via modal perturbation.

3.1 Modal strain energy-based damage localization

The modal strain energy of the j th sub-element $[a_j, a_{j+1}]$ associated with the i th mode of a Bernoulli-Euler beam before and after damage is given by (Cornwell *et al.* 1999)

$$MSE_{i,j} = \frac{1}{2} \int_{a_j}^{a_{j+1}} EI(x) \cdot \left(\frac{\partial^2 \varphi_i}{\partial x^2} \right)^2 dx \quad (21)$$

$$MSE_{i,j}^d = \frac{1}{2} \int_{a_j}^{a_{j+1}} EI^d(x) \cdot \left(\frac{\partial^2 \varphi_i^d}{\partial x^2} \right)^2 dx \quad (22)$$

where superscript d denotes damage, EI and φ_i are the flexural rigidity of the sub-element and the i th mode shape, respectively. Given that flexural rigidity after damage $EI^d(x)$ is unpredictable, the original flexural rigidity $EI(x)$ can be used as an approximation in Eq. (22). According to Shi and Law (1998), a normalized change ratio of the modal strain energy is taken as the damage location indicator

$$NMSECR_j^i = \frac{|MSE_{i,j}^d - MSE_{i,j}|}{MSE_{i,j}} / \max\left(\frac{|MSE_{i,j}^d - MSE_{i,j}|}{MSE_{i,j}}\right) \quad (23)$$

If more than one vibration mode is considered, the damage location indicator in the j th sub-element is defined as the average of $NMSECR_j^i$ for all the concerned modes.

$$NMSECR_j = \frac{1}{m} \sum_{i=1}^m NMSECR_j^i \quad (24)$$

3.2 Damage quantification

In damage detection studies, it is a common assumption that no mass change occurs after damage. The occurrence of damage in a beam can be represented by a change in the flexural rigidity

$$EI^d(x) = EI(x) + \Delta EI(x) = EI(x) + \sum_j \beta_j EI(x) \quad (-1 \leq \beta_j \leq 0) \quad (25)$$

where β_j is the stiffness reduction factor or damage index in the j th sub-element ($a_j \leq x \leq a_{j+1}$). It causes perturbations, which are typically small, in the i th eigenvalue λ_i^d and the i th mode shape $\varphi_i^d(x)$, compared with the undamaged beam (Shi *et al.* 2000, Fox 1968).

$$\lambda_i^d = \lambda_i + \Delta \lambda_i \quad (26)$$

$$\varphi_i^d = \varphi_i + \Delta \varphi_i = \varphi_i + \sum_{j \neq i} q_j \varphi_j \quad (27)$$

Then the damage-induced change in $MSE_{i,j}$ can be expressed as

$$\Delta MSE_{i,j} = MSE_{i,j}^d - MSE_{i,j} = \int_{a_j}^{a_{j+1}} [EI(x) \frac{\partial^2 \varphi_i}{\partial x^2} \frac{\partial^2 \Delta \varphi_i}{\partial x^2}] dx + \frac{1}{2} \int_{a_j}^{a_{j+1}} \Delta EI(x) \cdot (\frac{\partial^2 \varphi_i}{\partial x^2})^2 dx \quad (28)$$

The $\Delta MSE_{i,j}$ can also be expressed as

$$\begin{aligned} \Delta MSE_{i,j} &= \frac{1}{2} \int_{a_j}^{a_{j+1}} EI^d(x) (\frac{\partial^2 \varphi_i^d}{\partial x^2})^2 dx - \frac{1}{2} \int_{a_j}^{a_{j+1}} EI(x) (\frac{\partial^2 \varphi_i}{\partial x^2})^2 dx \\ &= \frac{1}{2} \int_{a_j}^{a_{j+1}} EI(x) (\frac{\partial^2 \varphi_i^d}{\partial x^2})^2 dx + \frac{1}{2} \int_{a_j}^{a_{j+1}} \beta_j EI(x) (\frac{\partial^2 \varphi_i^d}{\partial x^2})^2 dx - \frac{1}{2} \int_{a_j}^{a_{j+1}} EI(x) (\frac{\partial^2 \varphi_i}{\partial x^2})^2 dx \end{aligned} \quad (29)$$

According to the dynamics of the beam (Clough and Penzien 1993), the partial differential equation defining the eigensolutions is

$$\frac{\partial^2}{\partial x^2} [EI(x) \frac{\partial^2 \varphi_i}{\partial x^2}] - \lambda_i m(x) \varphi_i = 0 \quad (30)$$

Again, when the beam is subject to damage, the above-described equation with a small perturbation becomes

$$\frac{\partial^2}{\partial x^2} \left\{ [EI(x) + \Delta EI(x)] \cdot \frac{\partial^2 (\varphi_i + \Delta \varphi_i)}{\partial x^2} \right\} - (\lambda_i + \Delta \lambda_i) m(x) (\varphi_i + \Delta \varphi_i) = 0 \quad (31)$$

Substituting Eqs. (25) - (27) and (30) into Eq. (31), and neglecting small terms leads to

$$\frac{\partial^2}{\partial x^2} [EI(x) \sum_{j \neq i} q_j \frac{\partial^2 \varphi_j}{\partial x^2} + \Delta EI(x) \frac{\partial^2 \varphi_i}{\partial x^2}] - \lambda_i m(x) \sum_{j \neq i} q_j \varphi_j - \Delta \lambda_i m(x) \varphi_i = 0 \quad (32)$$

Pre-multiplying φ_j and computing the integral along the interval $[0, L]$ on both sides of Eq. (32), and considering the orthogonal condition

$$\int_L \varphi_j m(x) \varphi_i dx = 0 \quad (i \neq j) \quad (33)$$

the coefficient q_j can be computed as

$$q_j = \frac{1}{\lambda_i - \lambda_j} \int_L [\Delta EI(x) \frac{\partial^2 \varphi_j}{\partial x^2} \frac{\partial^2 \varphi_i}{\partial x^2}] dx \quad (34)$$

Supposing q_j sub-elements out of a total of N are damaged, the following damage equation can be obtained from Eqs. (28) - (29) and (34)

$$\begin{bmatrix} \chi_{11} & \chi_{12} & \cdots & \chi_{1m} \\ \chi_{21} & \chi_{22} & \cdots & \chi_{2m} \\ \vdots & \vdots & & \vdots \\ \chi_{m1} & \chi_{m2} & \cdots & \chi_{mm} \end{bmatrix} \begin{Bmatrix} \beta_1 \\ \beta_2 \\ \vdots \\ \beta_m \end{Bmatrix} = \begin{Bmatrix} \Delta MSE_{i,1} \\ \Delta MSE_{i,2} \\ \vdots \\ \Delta MSE_{i,m} \end{Bmatrix} \quad (35)$$

where

$$\begin{aligned} \chi_{kk} = & \sum_{j \neq i} \left[\frac{1}{\lambda_i - \lambda_j} \int_{a_k}^{a_{k+1}} EI(x) \frac{\partial^2 \varphi_j}{\partial x} \frac{\partial^2 \varphi_i}{\partial x} dx \right] \left[\int_{a_k}^{a_{k+1}} EI(x) \frac{\partial^2 \varphi_j}{\partial x} \frac{\partial^2 \varphi_i}{\partial x} dx \right] \\ & + \frac{1}{2} \int_{a_k}^{a_{k+1}} EI(x) \left(\frac{\partial^2 \varphi_i}{\partial x} \right)^2 dx - \frac{1}{2} \int_{a_k}^{a_{k+1}} EI(x) \left(\frac{\partial^2 \varphi_j}{\partial x} \right)^2 dx \end{aligned} \quad (36)$$

$$\chi_{kt} = \sum_{j \neq i} \left[\frac{1}{\lambda_i - \lambda_j} \int_{a_t}^{a_{t+1}} EI(x) \frac{\partial^2 \varphi_j}{\partial x} \frac{\partial^2 \varphi_i}{\partial x} dx \right] \left[\int_{a_t}^{a_{t+1}} EI(x) \frac{\partial^2 \varphi_j}{\partial x} \frac{\partial^2 \varphi_i}{\partial x} dx \right] \quad (37)$$

where $k, t = 1, 2, \dots, m$. In the WFEM, the eigenvalues λ and eigenvectors φ can be obtained directly from Eq. (17).

After the damage is located using the method described in Section 3.1, its severity can be qualified by solving the above-described damage matrix equation. The two-stage process, i.e., location and quantification, can effectively reduce the matrix size and minimize the computation cost. Notably, the flexural rigidity after damage $[EI(x) + \Delta EI(x)]$ rather than $[EI(x)]$ is used in the damage matrix equation. Therefore, the iteration computation adopted by Shi *et al.* (2000) is not required, which helps enhance detection efficiency.

3.3 Progressive damage detection

This study adopts a progressive damage detection strategy, in which a low-resolution structure model is first used to acquire the potential location and severity of damage, and a multi-resolution model with refinement in the suspected regions is then used to obtain more accurate estimation of the damage. Although this adaptive-scale strategy can theoretically be realized in the context of traditional FEM with effort of re-meshing the models and re-constructing the matrices, the novel WFEM provides considerable convenience and flexibility to dynamically change the modeling scale according to the needs in each step. A flowchart of the adaptive-scale damage detection process is shown in Fig. 2, which consists of the following main steps:

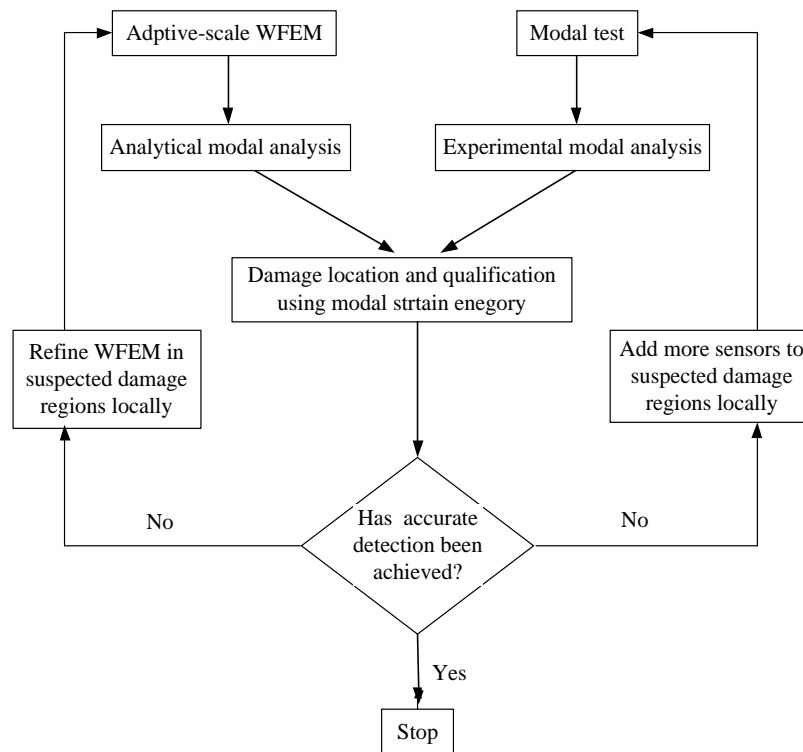


Fig. 2 Flowchart of adaptive-scale damage detection scheme

- Step 1: Arrange the sensors in the tested beam structure, measure the modal properties (i.e., mode shapes), and calculate the modal strain energy in each region;
- Step 2: Analyze the modal properties of the undamaged beam using the adaptive-scale WFEM, and then compute the modal strain energy in the corresponding regions;
- Step 3: Locate the suspected region by comparing the analytical and measured modal strain energies and then quantify the damage severity (However, damage quantification is not compulsory in this step. To reduce the computation cost, it can be carried out only in Step 6 after the damage is properly located);
- Step 4: Refine the WFEM by adding high-scale wavelet terms in the suspected damage regions, and then add more sensors in the corresponding regions of the tested beam;
- Step 5: Repeat Steps 1-4 until accurate estimations of the location and severity of the damage are achieved. As each considered region is divided into two equal-length sub-regions when refine the WFEM, this iterative progress can be stopped if the newly divided two sub-regions are all located as damage areas;
- Step 6: Quantify the damage severity based on the modal strain energy.

This progressive method is efficient in terms of computation and testing, in that (1) the structural model is refined only in the key locations; (2) the refinement process in the context of the WFEM is convenient due to its salient features; and (3) only a limited number of sensors need to be added in the critical regions.

4. Adaptive-scale damage detection

Numerical examples of a simply supported beam and a continuous beam are used to demonstrate the effectiveness of the adaptive-scale damage detection method. The material and section properties of these two beams are as follows: elastic modulus $E = 2$ GPa, density $\rho = 2500 \text{ kg/m}^3$, cross-sectional area $A = 0.005 \text{ m}^2$, and moment of inertia $I = 1.667 \times 10^{-4} \text{ m}^4$. Table 1 summarizes the three damage cases investigated in this numerical study. The first two involves a simply supported beam, while the third involves a two-span continuous beam. Different locations and severity of the damage are assumed in the three cases, where the location refers to the interval of damage, and the severity refers to the loss of flexural rigidity in the damage interval. In numerical simulations, the modal properties obtained from very densely meshed traditional FEMs are taken as the measurement results. In particular, the measurement error due to sensor noise is considered in Section 4.2 in order to check the robustness of the damage detection method in all the cases. Considering that only the lower mode shapes can be measured in real field testing, only the first mode shape is used in the examples without noise, while the first four mode shapes are used in the examples with noise. The damage detection results for each case are elaborated in this section.

Table 1 Damage scenarios considered in the numerical simulations

Structure	Damage Scenarios		Damage	
			Location	Severity (%)
A simply-supported beam	Case 1	Single damage	[5.25, 5.5]	20
	Case 2	Double damage	[1.0,1.5]	20
			[6.25,6.5]	20
A two-span continuous beam	Case 3	Double damage	[3.25,3.5]	20
			[12.5,12.75]	20

4.1 Examples without noise

Case 1 involves a simply supported beam structure subject to a single damage in the interval of [5.25, 5.5] with the severity of 20%. Fig. 3 shows the model refinement process, and Fig. 4 shows the damage identification results in each step. In the adaptive-scale damage detection process, a low-scale WFEM is used to simulate the original beam structure. The beam is modelled by eight cubic Hermite wavelet finite elements at scale 0, i.e., the shape functions of each element are approximated in wavelet space V_0 (as shown in Fig. 3). The corresponding number of DOFs at scale 0 is 18. The modal strain energy associated with the first mode shape is computed for eight beam elements. By comparing the difference between the simulated and “measured” results, the location and severity of damage can be estimated using the method described in Sections 3.1 and 3.2 (as shown in Fig. 4). Although the damage severity cannot be evaluated accurately due to the low-scale model, the suspected damage region, i.e., interval [5, 6], can be successfully identified at

scale V0. Subsequently, the WFEM is refined on the interval [5, 6] by lifting the wavelet scale, i.e., its shape function is represented by the wavelet approximation in space V1; meanwhile, one more measurement point at $x = 5.5$ is added in the modal testing, and thus the resolution of the measured mode shape is also refined in this region. As shown in Fig. 4, the damage location can be identified in a smaller sub-element region in step V1. Repeating the refinement and identification process allows for the more accurate estimations of location and severity of the damage through the iteration. Finally, the results at scales V2 and V3 show almost the same damage location, implying that the estimation converges and no further refinement is necessary. The quantification results of the damage severity in each step are also shown in Fig. 4. It is not surprising to see the relatively inaccurate estimation of the damage severity in a low-scale model, due to the inaccurate assumption of the damage location. However, the accuracy of quantification is effectively improved with the progressive refinement of the model, and it finally converges toward the real value in steps V2 and V3. It should be pointed out that the damage quantification results in Fig. 4 are for illustration. According to the procedure describe in Section 3.3, the damage severity needs to be quantified only when the damage location is best identified, i.e., in the last step in this case.

Considering the fact that the damage location is always unpredictable, the traditional FEM, if used in this case, should be uniformly meshed without the adaptive-scale technique. 32 beam elements with 66 DOFs are required in this way to accurately capture the damage in Case 1, where the single damage region consists of 1/32 of the whole beam. With the proposed adaptive-scale strategy, however, only 24 DOFs in step V3 are used in the WFEM to achieve the same accuracy level of damage detection. Furthermore, we do not need to specify the required model scale in advance, and the damage is located and quantified progressively.

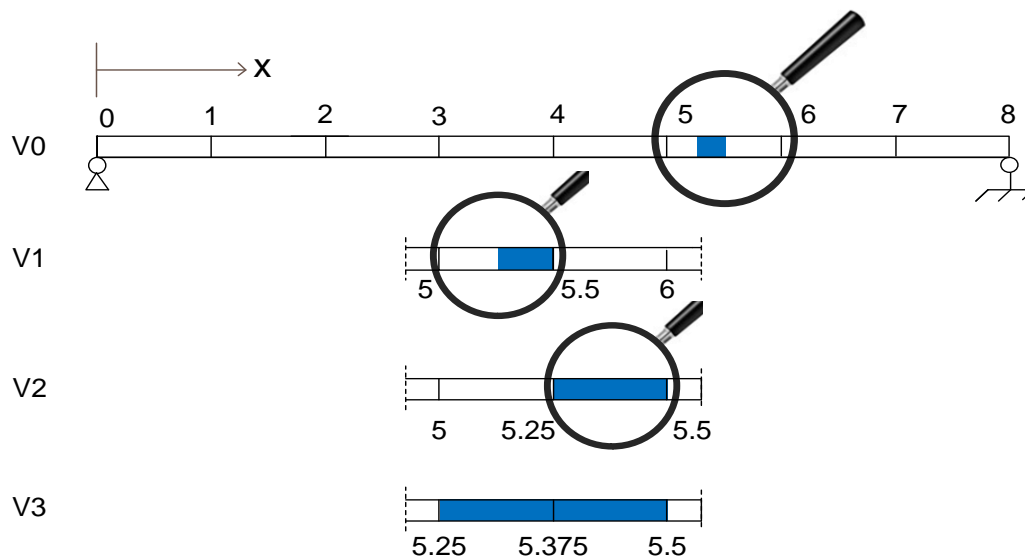


Fig. 3 Model refinement process in Case 1 (the shaded area represents the damage region)

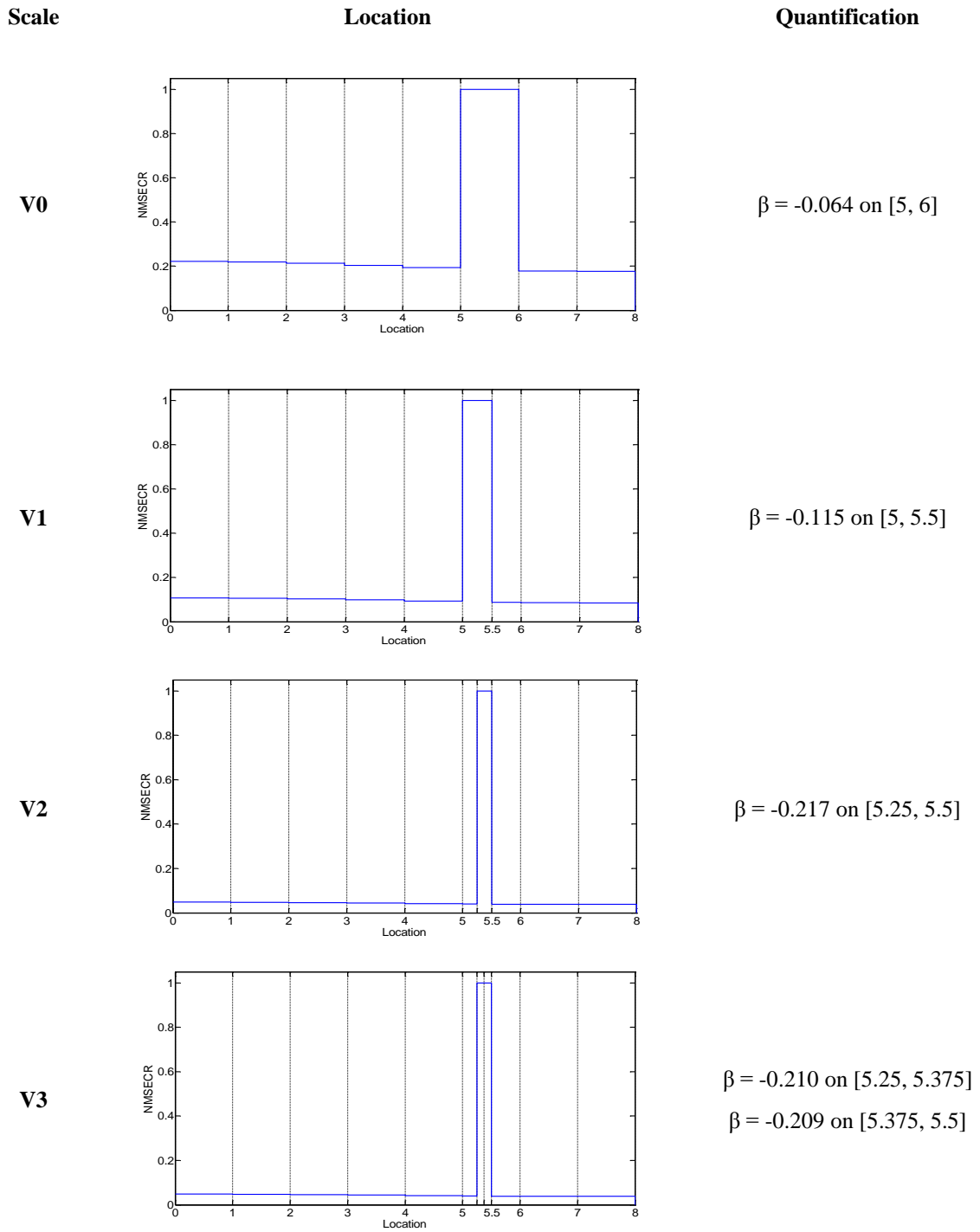


Fig. 4 Adaptive-scale damage identification results in Case 1

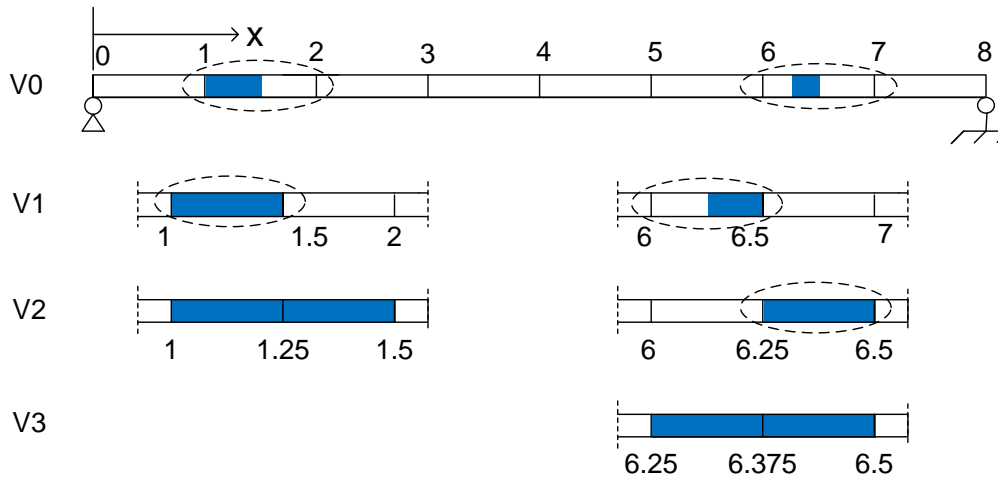


Fig. 5 Model refinement process in Case 2 (the shaded area represents the damage region)

Table 2 Adaptive-scale location and quantification of damage using WFEM

Scale	Case 1		Case 2		Case 3	
	Location	Severity (%)	Location	Severity (%)	Location	Severity (%)
V0	[5, 6]	6.4	[1, 2]	7.8	[3, 4]	5.4
			[6, 7]	5.2	[12, 13]	5.4
V1	[5, 5.5]	11.5	[1, 1.5]	21.7	[3, 3.5]	9.0
			[6, 6.5]	9.5	[12.5, 13]	9.0
V2	[5.25, 5.5]	21.7	[1, 1.25]	20.4	[3.25, 3.5]	21.2
			[1.25, 1.5]	20.5	[12.5, 12.75]	21.2
			[6.25, 6.5]	20.5		
V3	[5.25, 5.375]	21.0	[1, 1.25]	20.4	[3.25, 3.375]	20.6
			[1.25, 1.5]	20.4	[3.375, 3.5]	20.1
			[6.25, 6.375]	20.3	[12.5, 12.625]	20.1
			[6.375, 6.5]	20.2	[12.625, 12.75]	20.6

Case 2 involves a beam subject to double damage with the severity of 20%. The damage locations are described in Table 1, and the corresponding refinement process and the damage identification results are presented in Fig. 5 and Table 2, respectively. Following the same process, the locations and severities of the damage can be identified with progressively improved accuracy. As the left-hand damage consists of 1/16 of the entire beam, a good estimation is obtained in step

V1 and verified in step V2, and thus no further refinement is conducted in this region in the last step. In comparison, the right-hand damage is 1/32 of the beam length, and the relevant region is gradually refined until the last step V3. These demonstrate that the model scale can be adaptively adjusted according to the actual state of damage, and such adaptability of the proposed strategy can help achieve accurate results with minimized number of DOFs and computation cost in applications.

Fig. 6 shows the dimension and damage locations of a two-span continuous beam. The severity of two damages is also 20%, with one in the interval of [3.25, 3.5] and the other in [12.5, 12.75]. The corresponding damage identification results are summarized in Table 2. Again, both the locations and severities of the damages can be identified with progressively improved accuracy.

4.2 Examples with noise

In actual modal testing, the collected data are inevitably contaminated by measurement noise. This section examines the sensitivity of the proposed damage detection method to the error or uncertainty in the measured modal properties. The mode shape with measurement error is expressed by (Yan *et al.* 2010)

$$\bar{\Phi}_{rj} = \Phi_{rj}(1 + \eta\zeta_{rj}) \tag{38}$$

where $\bar{\Phi}_{rj}$ and Φ_{rj} are the “measured” and accurate mode shape components of the r th mode at the j th DOF, respectively; η is the measurement error level considered in the “measured” mode shapes; and ζ_{rj} is zero-mean Gaussian random variables. Five different levels of measurement error in mode shapes are considered: 1%, 2%, 3%, 4% and 5%. To reduce the influence of random measurement error on the experimental mode shapes in this case, the first four mode shapes are utilized in the damage detection process.

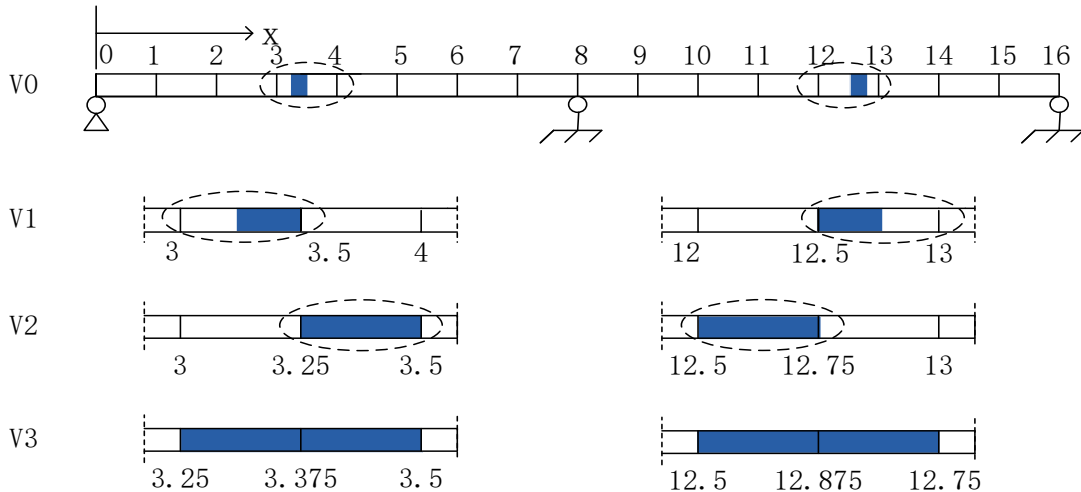


Fig. 6 Model refinement process in Case 3

The random measurement error is simulated using the Monte Carlo method, and each level of measurement error consists of 10000 Monte Carlo simulations. The statistical characteristics of the damage detection results are examined, e.g., the coefficient of variance (COV) of the estimated damage severity

$$COV = \frac{\sigma_a}{\bar{a}} \tag{39}$$

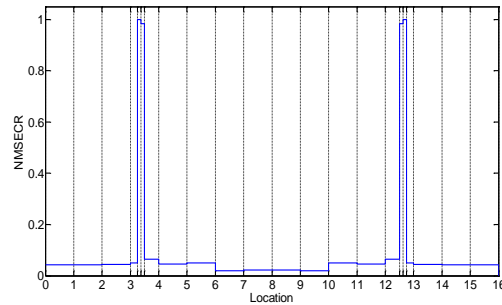
where \bar{a} and σ_a represent the mean and standard deviation of damage index ($NMSECR$ and β), respectively.

**Measurement
error level**

Location

Quantification

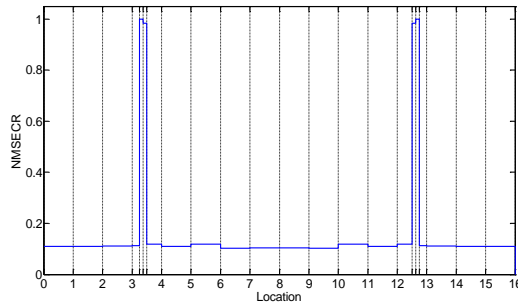
No error



$\beta = -0.206$ on [3.25, 3.375]
 $\beta = -0.201$ on [3.375, 3.5]

 $\beta = -0.201$ on [12.5, 12.625]
 $\beta = -0.206$ on [12.625, 12.75]

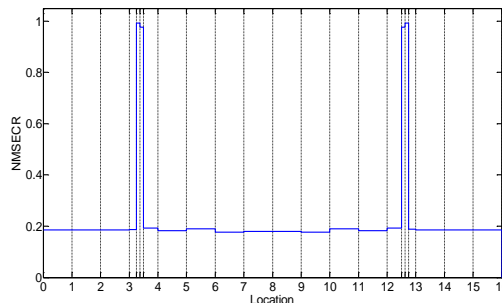
3% error



$\beta = -0.205$ on [3.25, 3.375]
 $\beta = -0.200$ on [3.375, 3.5]

 $\beta = -0.200$ on [12.5, 12.625]
 $\beta = -0.205$ on [12.625, 12.75]

5% error



$\beta = -0.205$ on [3.25, 3.375]
 $\beta = -0.200$ on [3.375, 3.5]

 $\beta = -0.200$ on [12.5, 12.625]
 $\beta = -0.205$ on [12.625, 12.75]

Fig. 7 Damage identification results under different noise levels at scale V3 in Case 3

Fig. 7 shows the damage detection results in the last step (i.e., at scale V3) of Case 3 with different levels of measurement error, where the normalized modal strain energy $NMSECR$ and the estimated damage severity β are the ensemble average of 10000 samples. The average results can well reflect the locations and severity of the double damage, but the presence of measurement error affects the average $NMSECR$ of undamaged areas, which increases with the measurement error level. In general, no significant changes can be observed among three measurement error levels, implying that the impact of random measurement error can be minimized by averaging results from a sufficient number of measurements. However, apparently changes in COV can be observed with the increasing measurement error level. Figs. 8 and 9 show the COVs of the estimated damage indices at the different scales in Case 1 and Case 3. A higher COV in the results implies greater uncertainty in a single sample or more samples required to obtain accurate estimation. In general, the uncertainty in the detection results increases with the measurement error level. In particular, the same error level results in a greater COV at a high wavelet scale, indicating that a high-scale WFEM is more sensitive to measurement noise. Similar observations on the estimation of the damage locations can be made.

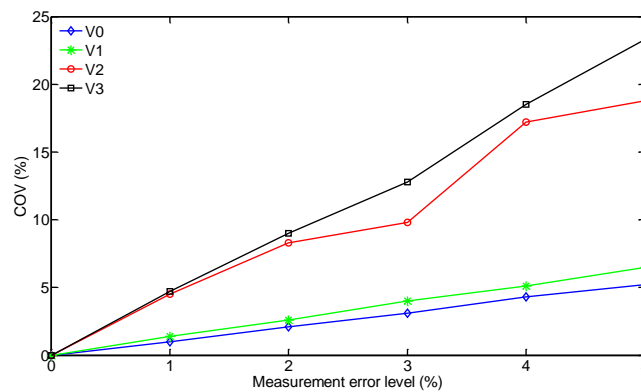


Fig. 8 COV of the estimated damage index of the simply-supported beam in Case 1

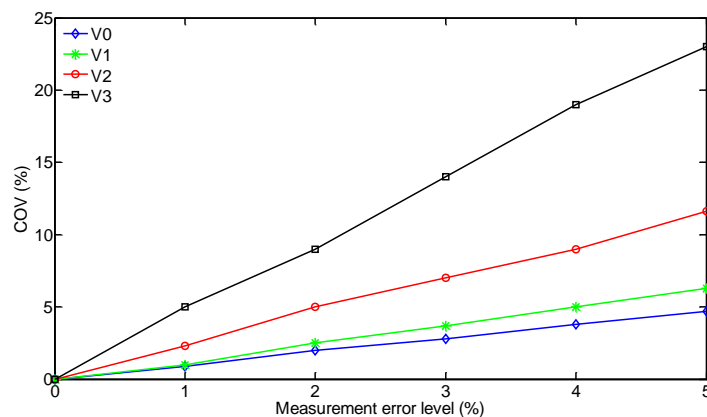


Fig. 9 COV of the estimated damage index of the continuous beam in Case 3

5. Conclusions

An adaptive-scale damage detection approach using the second-generation cubic Hermite wavelet finite beam element is proposed in this study. The dynamic equations and modal properties of beam structures are derived in the context of the WFEM. In particular, the adopted WFEM can seamlessly connect to or even be used to refine traditional beam finite elements. Using modal strain energy as a damage indicator, structural damage can be located and quantified in a progressive manner—a coarse WFEM is used to identify the likely damage region first; whereas gradually lifted WFEMs with local refinement are used to estimate the accurate location and severity of the damage. The superior multi-resolution and localization properties of the WFEM enable a convenient change of modeling scales in the damage detection process.

Numerical examples of a simply supported beam and a two-span continuous beam are analyzed with different damage scenarios. The results demonstrate that the adaptive-scale strategy can progressively and accurately locate and quantify the damage in beam structures in different cases. In particular, the impact of measurement noise on the identification results is also assessed via Monte Carlo simulations. The detection accuracy is more sensitive to the noise at a relatively higher scale. In general, the proposed damage detection strategy is very efficient, in terms of the number of DOFs, number of sensors, and computation effort.

Modal strain energy is adopted to showcase the WFEM-based adaptive-scale damage detection strategy. It should be noted that some limitations had been found in the practical implementation of modal strain energy-based damage detection methods, such as mass normalization of measured mode shapes, ill-positioning of sensitivity matrix and so on (Ren and De Roeck 2002). As the purpose of this paper is to develop a WFEM-based adaptive-scale damage detection strategy which is very efficient in terms of the number of DOFs in structural models and sensors in modal tests, how to overcome these limitations is out of the main scope of this paper even though they are certainly very important issues that require further investigations by SHM community. Besides, various damage detection techniques that have been developed in the context of traditional FEM can also be used in conjunction with the multi-scale WFEM. Apart from beam elements, other types of WFEMs were developed in the past, and they warrant further research for their applications in damage detection.

Acknowledgments

The authors are grateful for the financial support from the Hong Kong Polytechnic University through the research projects (Project No. A-PL42 and G-YL31). Findings and opinions expressed here, however, are those of the authors alone, not necessarily the views of the sponsor.

References

- Amaratunga, K. and Sudarshan, R. (2006), "Multi-resolution modeling with operator-customized wavelets derived from finite elements", *Comput. Method Appl. M.*, **195**, 2509-2532.
- Averbuch, A.Z., Zheludev, V.A. and Cohen, T. (2007), "Multiwavelet frames in signal space originated from Hermite splines", *IEEE T. Signal Proces.*, **55**(3), 797-808.
- Bakhary, N., Hao, H. and Deeks, A.J. (2010), "Structure damage detection using neural network with

- multi-stage substructuring”, *Adv. Struct. Eng.*, **13**(1), 95-110.
- Balageas, D., Fritzen, C.P. and Guemes, A. (2006), *Structural health monitoring*, ISTE USA, Newport Beach, CA, USA.
- Chen, W.H. and Wu, C.W. (1995), “Spline wavelets element method for frame structures vibration”, *Comput. Mech.*, **16**, 1-21.
- Chen, X.F., Zi, Y.Y., Li, B. and He, Z.J. (2006), “Identification of multiple cracks using a dynamic mesh-refinement method”, *J. Stain Anal. Eng.*, **41**, 31-39.
- Chui, C.K. (2009), *An introduction to wavelets*, Posts and Telecom Press, Beijing, China.
- Clough, W. and Penzien, J. (1993), *Dynamics of structures* (3rd Ed.), McGraw-Hill, New York.
- Cornwell, P., Doebling, S.W. and Farrar, C.R. (1999), “Application of the strain energy damage detection method to plate-like structures”, *J Sound Vib.*, **224** (2), 359-374.
- Ding, Y.L., Li, A.Q., Du, D.S. and Liu, T. (2010), “Multi-scale damage analysis for a steel box girder of a long-span cable-stayed bridge”, *Struct. Infrastruct. E.*, **6**(6), 725-739.
- Doebling, S.W., Farrar, C.R., Prime, M.B. and Shevitz, D.W. (1996), *Damage identification and health monitoring of structural mechanical systems from changes in their vibration characteristics: a literature review*, Report No. LA-13070-MS, Los Alamos National Laboratory, Los Alamos, NM, USA.
- Fan, W. and Qiao, P.Z. (2011), “Vibration-based damage identification methods: a review and comparative study”, *Struct Health Monit.*, **10**(1), 83-111.
- Fox, R.L. and Kapoor, M.P. (1968), “Rate of change of eigenvalues and eigenvectors”, *AIAA J.*, **6**(12), 2426-2429.
- Guan, H. and Karbhari, V.M. (2008), “Improved damage detection method based on element modal strain damage index using sparse measurement”, *J. Sound Vib.*, **309**(3-5), 465-494.
- Han, J.G., Ren, W.X. and Huang, Y. (2005), “A multivariable wavelet based finite element method and its application to thick plates”, *Finite Elem. Anal. Des.*, **41**, 821-833.
- Han, J.G., Ren, W.X. and Huang, Y. (2006), “A spline wavelet finite-element method in structural mechanics”, *Int. J. Numer. Meth. Eng.*, **66**, 166-190.
- He, W.Y., Ren, W.X. and Yang, Z.J. (2012) “Computation of plane crack stress intensity factors using trigonometric wavelet finite element methods”, *Fatigue Fract. Eng. M.*, **35**, 732-741.
- He, W.Y. and Ren, W.X. (2012), “Finite element analysis of beam structures based on trigonometric wavelet”, *Finite Elem. Anal. Des.*, **51**, 59-66.
- He, W.Y. and Ren, W.X. (2013a), “Adaptive trigonometric hermite wavelet finite element method for structural analysis”, *Int. J. Struct. Stab. Dy.*, **1**, 1350007.
- He, W.Y. and Ren, W.X. (2013b), “Trigonometric wavelet-based method for elastic thin plate analysis”, *App. Math. Model.*, **37**, 1607-1617.
- He, W.Y. and Zhu, S. (2013), “Progressive damage detection based on multi-scale wavelet finite element model: numerical study”, *Comput. Struct.*, **125**, 177-186.
- Ko, J., Kurdila, A.J. and Pilant, M.S. (1995), “A class of finite element methods based on orthonormal, compactly supported wavelets”, *Comput. Mech.*, **16**, 235-244.
- Kim, H.M. and Bartkiewicz, T.J. (1997), “A two-step structural damage detection approach with limited instrumentation”, *J. Vib. Acoust.*, **119**(2), 258-264.
- Kim, J.T., Park, J.H., Hong, D.S. and Park, W.S (2010), “Hybrid health monitoring of prestressed concrete girder bridges by sequential vibration-impedance approaches”, *Eng. Struct.*, **32**(1), 115-128.
- Li, B., Chen, X.F., Ma, J.X. and He, Z.J. (2005), “Detection of crack location and size in structures using wavelet finite element methods”, *J. Sound Vib.*, **285**, 767-782.
- Li, Z.X., Chan, T.H.T., Yu, Y. and Sun, Z.H. (2009), “Concurrent multi-scale modeling of civil infrastructures for analyses on structural deterioration, Part I: Modeling methodology and strategy”, *Finite Elem. Anal. Des.*, **45**, 782-794.
- Mallat, S. (1988), *Multi-resolution representation and wavelets*, Ph.D. Dissertation, University of Pennsylvania, Philadelphia, PA.
- Perera, R. and Ruiz, A. (2008), “A multistage FE updating procedure for damage identification in large-scale structures based on multi-objective evolutionary optimization”, *Mech. Syst. Signal Pr.*, **22**,

- 970-991.
- Ren, W.X. and De Roeck, G. (2002), "Discussion of "Structural Damage Detection from Modal Strain Energy Change" by z. Y. Shi, S. S. Law, and L. M. Zhang", *J. Eng. Mech. - ASCE*, **128**, 376-377.
- Redjienski, M., Krawczuk, M. and Palacz, M. (2011), "Improvement of damage detection methods based on experimental modal parameters", *Mech. Syst. Signal Pr.*, **25**(6), 2169-2190.
- Shi, Z.Y. and Law, S.S. (1998), "Structural damage localization from modal strain energy change", *J. Sound Vib.*, **218** (5), 825-844.
- Shi, Z.Y., Law, S.S. and Zhang, L.M. (2000), "Structural damage detection from modal strain energy change", *J. Eng. Mech. - ASCE*, **126** (12), 1216-1223.
- Shi, S.Y., Law, S.S. and Zhang L.M. (2002), "Improved damage quantification from elemental modal strain energy change", *J. Eng. Mech.- ASCE*, **128**(5), 521-529.
- Sohn, H., Farrar, C.R., Hemez, F.M., Shunk, D.D., Stinemates, D.W. and Nadler, B.R. (2004), *A review of structural health monitoring literature 1996-2001, Report No. LA-13976-MS*, Los Alamos National Laboratory, Los Alamos, NM, USA.
- Sudarshan, R. and Amaratunga, K. (2003), "Hierarchical solution of eigenvalue problems using finite element multi-wavelets", *Proceedings of the VII International Conference on Computational Plasticity (COMPLAS 2003)*, Barcelona.
- Sweldens, W. (1996), "The lifting scheme: a custom-design construction of biorthogonal wavelets", *Appl Comput Harmon A.*, **3**, 186-200.
- Wang, Y.M., Chen, X.F., He, Y.M. and He, Z.J. (2011), "The construction of finite element multi -wavelets for adaptive structural analysis", *Int. J. Numer. Meth. Bio.*, **27**, 562-584.
- Xiang, J.W., Chen, X.F., He, Y.M. and He, Z.J. (2006). "Identification of crack in a beam based on finite element method of B-spline wavelet on the interval", *J. Sound Vib.*, **296**,1046-1052.
- Xiang, J.W. and Liang, M. (2011), "Multiple damage detection method for beams based on multi-scale elements using Hermite cubic spline wavelet", *Comp Model Eng.*, **73**(3), 267-298.
- Yan, W.J., Huang, T.L. and Ren, W.X. (2010), "Damage detection method based on element modal strain energy sensitivity", *Adv. Struct. Eng.*, **13**, 1075-1088.
- Yan, W.J. and Ren, W.X. (2012), "Statistic structural damage detection based on the closed-form of element modal strain energy sensitivity", *Mech. Syst. Signal Pr.*, **28**, 183-194.
- Zienkiewicz, O.C. and Taylor, R.L. (1961), *The finite element method* (4th Ed.), McGraw-Hill Book Company, London.